Oxidative dissolution of NiO in aqueous electrolyte: an impedance study

Matteo Bonomo[a]*, Gaia Naponiello, Danilo Dini[a]

[a] Dept. of Chemistry, University of Rome "La Sapienza", p.le Aldo Moro 5, 00185 Rome, Italy

Abstract

The present contribution reports on the analysis of the electrochemical properties of screen-printed nickel oxide (NiO) in aqueous electrolyte when NiO is in the configuration of thin film (thickness, $l \leq 7$ μm). This type of NiO samples presents mesoscopic morphology. The latter characteristic combined to the intrinsic electroactivity of the oxide leads to the observation of proportionality between NiO thickness and current density. In particular, NiO undergoes two distinct processes of oxidation with reversible features in aqueous media. These redox processes occur in the solid state and, as such, involve mass/charge transfer between the NiO electrode and the electrolyte. On the other hand, the electrochemical oxidation of NiO is accompanied by the progressive chemical dissolution of the oxide when the latter is in the oxidized state. This is a consequence of the elevated content of stored charge on NiO surface when it interfaces a high polarity solvent like water. In the present work we have considered electrochemical impedance spectroscopy (EIS) for the investigation of the charge transfer/transport properties of NiO during the simultaneous occurrence of chemical and electrochemical processes. The study proposes models of electrical circuits for analyzing the interfacial phenomena involved in the aqueous oxidation of NiO.

Keywords: nickel oxide; electrochemistry; nanostructured electrode; impedance spectroscopy; equivalent circuit

* To whom correspondence should be addressed, *email*: matteo.bonomo@uniroma1.it

1. Introduction

Nickel oxide (NiO) is a *p*-type semiconducting material with bandgap width $E_g > 3.5$ eV [1]. The interesting electrical transport properties [2–9] combined to its chemical stability [10] and redox photoactivity [11–19] render nickel oxide suitable for a variety of electrochemical applications like energy storage [20–22], electrochromic windows [23–33], solar energy conversion in dye-sensitized solar cells (DSCs) [34,35] and perovskites solar cells [36,37]. Thin films of NiO are electroactive in the solid state and can act then as a charge storage system.[38,39] The diversity of the applicative finalities which NiO is destined to requires the adoption of different methods of preparation. Such a demand of diversification leads to the attainment of NiO in various shapes, morphologies, configurations as well as chemical compositions. Among the various methods of preparation of NiO electrodes for photo-electrochemical applications [13,40–48], we considered screen-printing [15,49], i.e. a method of physical deposition that employs NiO nanoparticles (NPs) dispersed in a spreadable viscous paste as precursor. The main advantages of screen-printing deposition are the scalability and the possibility of depositing uniform and homogeneous films of NiO with nanostructured features onto supporting substrates utilizing a simple and cost-effective experimental set-up. Such a deposition technique affords NiO films with electrical connectivity between the constituent NPs throughout the whole film and warrants the efficacious electrical contact at the NiO/substrate interface[50]. This is because the precursor containing NiO NPs is brought to a temperature sufficiently high (i.e. 450 °C) to sinter the NPs and warrant the electrical percolation between these[51,52]. Such a thermal treatment affords electrodes with nanostructured morphology, large surface area and good mechanical adhesion on a conductive substrate. Due to the spread use of nanostructured cathodes for the water-based (photo)electrochemical applications of water splitting[53–58], and dye-sensitized solar cells with aqueous electrolytes[59–63], it is believed that the fundamental study of the processes of charge transfer and current transport through nanostructured/mesoporous NiO films with thickness $l \leq 7$ μm,

[16,17,49] during oxidative chemical dissolution in aqueous electrolytes [16,64,65] would be relevant. As a matter of fact, it is of primary importance to individuate which alterations of the charge transport properties are introduced in nanostructured NiO electrodes under ordinary operative conditions when the electrolyte is protogenic.[59] The analysis of the electrical parameters characterizing the electrochemical behaviour of NiO electrodes would render possible the scrutiny of the ongoing processes of electrochemically induced dissolution of NiO in aqueous electrolyte. In doing so, we have considered the potentiodynamic techniques of cyclic voltammetry (CV)[50] and electrochemical impedance spectroscopy (EIS)[66–68]. In the plethora of works about NiO electrochemistry[69–76] the present study tackles for the first time the problem of how to characterize and model a non homogeneous, mesoscopic electrode of screen-printed NiO when the system is in electroactive state and undergoes an electrochemically activated process of dissolution in aqueous electrolyte. In this context the aspect of anodic evolution of O_2 at NiO electrodes with electrocatalytic features is not considered[77–79].

2. Experimental Section

2.1 Preparation of NiO electrodes

The preparation of the NiO paste, i.e. the precursors for screen-printing deposition, has been performed by following the procedural scheme previously reported in ref. 17 for paste there denominated P3 (Table 1). All chemicals here utilized were purchased from Sigma-Aldrich or Fluka. The reactants were at the highest degree of purity available and were then employed without any further purification. In brief, the starting mixture is an ethanol solution of NiO nanoparticles (variable diameter, ø = 20-50 nm), ethylcellulose, α-terpineol and concentrated hydrochloric acid (1 mL).

Step 1	6g of NiO nanopowders are grinded with 1mL of concentrated HCl acid for 5 min (final volume of mixture: 1 mL)
Step 2	Addition of 1mL of H_2O to the mixture obtained after Step 1 and grinding for 1 min. This succession is repeated 5 times (final volume of mixture: 6 mL)
Step 3	Addition of 1mL of ethanol to the mixture of Step 2 and grinding for 1 min. This succession is repeated 15 times (final volume of the mixture: 21 mL)
Step 4	Addition of 2.5mL of ethanol to the mixture of Step 3. This succession is repeated 6 times (final volume of the mixture: 36 mL)
Step 5	Transfer of the paste of Step 4 to a beaker using 100 mL of ethanol (final volume of the mixture: 136 mL)
Step 6	The mixture of Step 5 is stirred 1 min, successively sonicated for 2 min and finally stirred again for 1 min
Step 7	Addition of terpineol (20 g)
Step 8	The mixture of Step 7 is stirred 1 min, successively sonicated for 2 min and finally stirred again for 1 min
Step 9	Addition of a solution of ethyl cellulose to the mixture of Step 8. The added solution is formed by adding 3 g of ethyl cellulose in 30g of a 10% v/v solution of ethanol in aqueous solvent
Step 10	The mixture of Step 9 is stirred 1 min, successively sonicated for 2 min and finally stirred again for 1 min. This succession of 4 min is repeated 3 times
Step 11	Slow evaporation of the volatile components of the resulting mixture: The mixture of Step 10 is placed on hot plate at 50°C for 9 hours. After then the NiO nanoparticles paste is cooled down to ambient temperature and ready for being utilized in the screen-printing mode of deposition

Table 1. Procedure of preparation of the precursor-paste utilized to screen-print the electrodes of NiO here characterized.

The solution thus obtained was slowly heated at 50 °C to give a viscous slurry that could be easily spread onto conductive FTO covered glass panels (item no. TCO227 from Solaronix). Paste spreading was done *via* screen-printing through a 90.48 T mesh screen. Prior to paste spreading, the FTO-covered glass panel was cleaned in

ultrasonic bath (soapy water, acetone and isopropyl alcohol for 15 minutes each) to remove possible impurities and contaminants adsorbed on the transparent substrate. The as deposited slurry was kept at 110°C in the first 15 minutes of the thermal treatment to remove water molecules eventually adsorbed on the deposited layers. In the second stadium of the thermal treatment the system is brought to the maximum temperature of 450 °C at the rate of 15 °C/min. The deposit is maintained for 30 minutes at the chosen value of maximum temperature. At 450 °C the film loses any viscous consistency and sintering of NiO nanoparticles takes place. The selected combination of ramp rate, maximum temperature of processing and duration of the whole thermal treatment allows the creation of a conductive system constituted by NiO with the desired open and nanostructured morphology (Figure 1). Moreover, the adopted thermal treatment prevented also the full coalescence of the nanoparticles. Such an effect would have produced the unwanted deposition of compact films. Sintering of NiO nanoparticles at 450 °C leads to the necking of the NiO nanoparticles. The occurrence of necking allows the formation of a percolation path through which charge carriers deliver the electrical current. The experimental details for the physical characterization of mesoporous NiO electrodes have been reported by our research group in previously published papers [15–17,49,80].

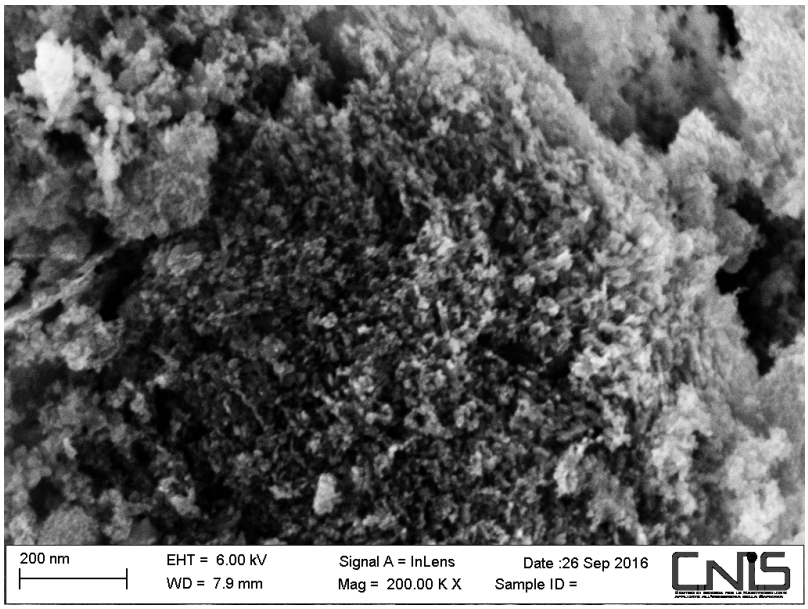

Figure 1. SEM images of the surface morphology of screen-printed NiO electrode (l = 2 μm).

2.2 Electrochemical characterization of screen printed NiO electrodes

Screen-printed NiO films on glass/FTO substrates were employed as working electrodes in three-electrode cells. A Pt wire and Ag/AgCl served as counter electrode and reference electrode, respectively. The aqueous electrolyte had the composition 0.2 M KCl, 0.01 M KH_2PO_4 and 0.01 M K_2HPO_4. In the paper the potential values are referred to the redox couple Ag/AgCl when not differently specified. CVs and EIS profiles were recorded with the potentiostat/galvanostat Autolab PGSTAT12® driven by the Autolab software Nova 1.9. EIS data were recorded within the frequency range $1*10^{-1}$–$1*10^{5}$ Hz with an amplitude of the potential perturbation of 10^{-2} V. The alternating potential we imposed to the cell was applied on going from the highest to the lowest frequency of oscillation. The EIS data were fitted with the software *Z*-View-3.3 (from Scribner Associates).

3. Results and Discussion

3.1 Electrochemical behavior of screen-printed NiO electrodes

The CVs of screen-printed NiO electrodes in water electrolyte presented two broad peaks (Figures 2), as commonly found for mesoporous samples.[13,14,16,17,37] Since the current density is generally proportional to the thickness of mesoporous NiO (Figures 2, left frames and Figure 3, *vide infra*), we evince that screen-printed NiO represents the actual electroactive species that originates the recorded voltamograms. These refer to the solid state oxidation of the NiO electrode according to the processes [40,65,81,82]:

$$NiO(H_2O)_p \rightarrow NiO(OH)(H_2O)_{p-1} + e- + H^+ \qquad \{1\}$$

$$NiO(OH)(H_2O)_{p-1} \rightarrow NiO(OH)_2(H_2O)_{p-2} + e- + H^+ \qquad \{2\}$$

in which pristine NiO in aqueous electrolyte is described as an hydrated systems and the Ni(II) centres are formally oxidized to Ni(III) and Ni(IV) in a consecutive way (succession of Eqs. 1 and 2). These reaction are characteristic of the electrochemistry of NiO in aqueous electrolyte regardless of the method of NiO synthesis/deposition [17,40,83]. The two peaks of NiO oxidation (labelled as **I** and **II** in the right frames of Figures 2) are linear with CV scan rate in aqueous environment.[37] This correlation indicates that the two observed processes of NiO oxidation are surface confined with both oxidized and reduced forms localized on the NiO electrode surface.[84]

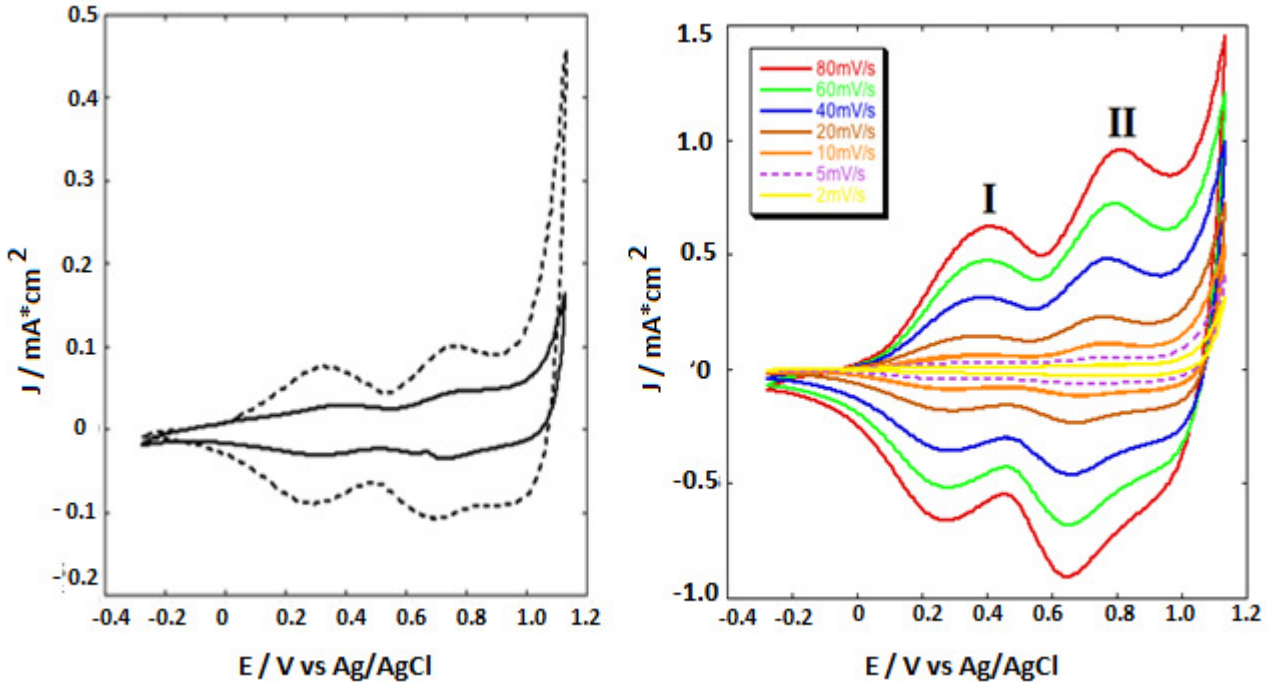

Figure 2. Left: CVs of screen-printed NiO thin films at the scan rate of 10 mV s^{-1} (full line: l = 2µm; dotted line: l = 6 µm). Right: CVs conducted at different scan rates for the NiO film with l = 6 µm. Electrolyte: 0.2 M KCl in water buffered by the acid-base couple 0.01 M KH_2PO_4 / 0.01 M K_2HPO_4.

The amplitude of the current peak is controlled by the surface concentration of Ni(II), i.e. the starting species of the redox oxidation. The redox process we observe is characterized by a rate determining step consisting in the oxidation of the Ni(II) sites localized on the surface of the electrode but not inside the thin film.[47] This is equivalent to say that the oxidation of Ni(II) does not involve the internal Ni(II) centers present in the bulk of the mesoporous oxide. This is principally a consequence of the high repulsive interaction the NiO film would have to sustain if the charge compensating ions are also inserted in the bulk of NiO and not only localized on the surface as actually occurs[39]. NiO in the pristine version contains surface states with Ni(III) centres as predicted by the most common theories on the

origin of the interfacial potential at an electrochemical double layer.[85] The Ni(III) centers in pristine NiO are mostly surface localized to compensate the rupture of the symmetry which occurs in passing from bulk to surface[47]. Moreover, surface localized Ni(III) sites stabilize the NiO/electrolyte interface as a consequence of the saturation of the dangling bonds at oxide surface. Along the same voltametric profile the amplitude of peak II is generally higher than that of peak I, regardless the thickness (Figure 3) of the NiO film.[17,40,83] From this finding, we deduce that Ni(III) surface concentration prior to the oxidation step II (Eq. 2) is larger than that of Ni(II) prior to the oxidation step I (Eq.1). Interestingly, the current amplitude of the thicker film is only two times the one of the thinner film. This leads to hypothesize that the thicker is less uniformly porous than the thinner one. At this regard, we determined the charge exchanged by NiO films with different thickness through the integration of the amperometric curves recorded at the potential of first oxidation of NiO when the metal oxide is in contact of an aqueous electrolyte (process I, Figure 2-left frame). Such a determination allows the evaluation of eventual differences of electroactive area per unit thickness of NiO films. Under these circumstances the charge that is exchanged by NiO during its potentiostatic oxidation is not heavily affected by the simultaneous process of chemical dissolution since the dissolved oxidized species based on Ni(III) are not further oxidized during process I (Eq.1). Moreover, the electrochemical process I, i.e. the process of solid state oxidation of NiO at lower potential, is a surface confined process in aqueous electrolyte[40]. As a such, the phenomenon of back diffusion of the dissolved product(s) based on Ni(III)

(Eq.1) results to be relatively slow and ineffective on the kinetics of the first electrochemical oxidation of NiO. The data of integrated charge during first oxidation of NiO are presented in Table 2.

s.r. /mV s^{-1}	2	5	10	20	40	60	80
l / µm							
2	**11.89** (5.94)	**11.53** (5.76)	**9.17** (4.58)	**9.74** (4.87)	**10.60** (5.30)	**10.50** (5.25)	**10.32** (5.16)
6	**28.64** (4.77)	**22.92** (3.82)	**22.92** (3.82)	**24.35** (4.06)	**26.50** (4.42)	**26.26** (4.38)	**25.78** (4.30)

Table 2. Values of charge (Q, in C cm^{-2}) exchanged per unit area by screen-printed NiO electrodes with variable thickness (*l*) during the occurrence of the oxidation process of Eq.1 (*vide supra*). In parentheses the value of the charge exchanged per unit area and unit thickness (Q′ in C cm^{-2} μm^{-1}) of NiO electrode is reported. The densities of exchanged charge have been calculated at seven different values of scan rate, s.r., and in potentiostatic conditions when E_{appl} = 0.34 V *vs* Ag/AgCl. The charge densities NiO exchanges potentiostatically during the first process of oxidation (Eq.1) are 5.19 and 4.33 C cm^{-2} μm^{-1} for 2 and 4 µm thick film, respectively.

Data in Table 2 show that the integrated charge depends on both scan rate and film thickness. The charge exchanged per unit volume of NiO film is generally larger for the thinner film with respect to thicker one (about 20 % larger) irrespective of the scan rate. This fact is mainly ascribed to the variation of porosity of the NiO film in passing from 2 to 6 µm of thickness. Data of Table 2 indicate also unequivocally that the thinner film of NiO presents the larger surface area with respect to the thicker sample. This conclusion is somehow supported by the fact that the impedance spectra of the thinner electrode of NiO are better modelled by an equivalent circuit that

212 includes the electrical parameters of FTO/electrolyte interface. This is equivalent to
213 say that the thinner film of screen-printed NiO does not coat uniformly the FTO
214 substrate (*vide infra*). When the dependence of the integrated charge on scan rate
215 (s.r.) is analysed, a not univocal trend of the charge density Q *vs* s.r. is observed
216 (Table 2). The maximum value of exchanged charge is determined at 40 mV s^{-1} for
217 both NiO electrodes which differ solely in thickness (Table 2). The existence of an
218 optimum value of exchanged charge indicates that the process I of NiO oxidation is
219 complicated by the occurrence of simultaneous reactions having different kinetics.
220 Since Q (and Q′) increases steadily within the s.r. range 5-40 mV s^{-1}, it is believed
221 that at the lowest scan rates (except 2 mV s^{-1}) the chemical dissolution of mesoporous
222 NiO is fast enough to diminish the amount of electroactive material on the electrode
223 surface when the electrode is under oxidative polarization. This is equivalent to say
224 that a prolonged time of anodic polarization better evidences the occurrence of NiO
225 dissolution. In fact, when screen-printed NiO is kept in a not polarized state and gets
226 immersed in the same electrolyte of the experiments in Figure 2, no
227 detachment/dissolution of NiO is observed. This is confirmed by the overlap of the
228 voltammetric profiles of the NiO electrode previously immersed in the electrolyte and
229 untreated NiO. Therefore, there is no variation of the charge of oxidation for NiO
230 electrodes upon variation of the time of immersion in aqueous electrolyte when NiO
231 is in the not polarized state. When the s.r. exceeds 40 mV s^{-1} the surface and volume
232 densities of exchanged charge diminish again despite of the fact that the durations of
233 anodic polarization of NiO are now shorter with respect to the voltammetries

234 conducted at slower scan rates. The reason of such a behaviour could be ascribed to
235 the kinetic limitation imposed by the movement of charge compensating ions towards
236 the surface of oxidized NiO when the rate of NiO oxidation becomes too high with
237 respect to the rate of migration of the charge compensating ions. At this concern, the
238 mechanism of charge compensation during NiO oxidation would include also the
239 arrival of anions from the electrolyte (as in case of NiO oxidation in non aqueous
240 solvents)[39] in addition to the (relatively faster) removal of protons from the
241 hydrated surface of NiO (Eqs. 1 and 2).
242 As far as the presence of Ni(III) is concerned, its presence in the pristine state of NiO
243 samples has been ascertained by means of X-ray photoelectron spectroscopy (XPS) in
244 a recent study from our group[86]. Such a finding is in accordance with the results
245 obtained from the XPS analysis of mesoporous NiO films deposited via rapid
246 discharge sintering [43,65]. The importance of the acknowledgment of the presence
247 of Ni(III) states in the pristine film of NiO resides on the fact that the Ni(III)/Ni(II)
248 ratio defines the actual stoichiometry of the NiO film and controls its electronic
249 conductivity and optical properties. The Ni(III)/Ni(II) ratio is related to the extent of
250 porosity of the film ($\approx 21.5\ m^2\ g^{-1}$ for screen-printed samples)[87] and augments with
251 the increase of NiO surface exposition.
252 The continuous repetition of the electrochemical cycles within the potential range of
253 NiO oxidation in aqueous electrolyte (Figures 3 and 4) gives the progressive
254 dissolution of screen-printed NiO electrode as previously verified with the NiO
255 samples prepared differently[17,64,65]. The electrochemically induced dissolution of

NiO is observed as the continuous, progressive thinning of the voltammograms associated to the oxidation of NiO upon repetition of the potential scan.

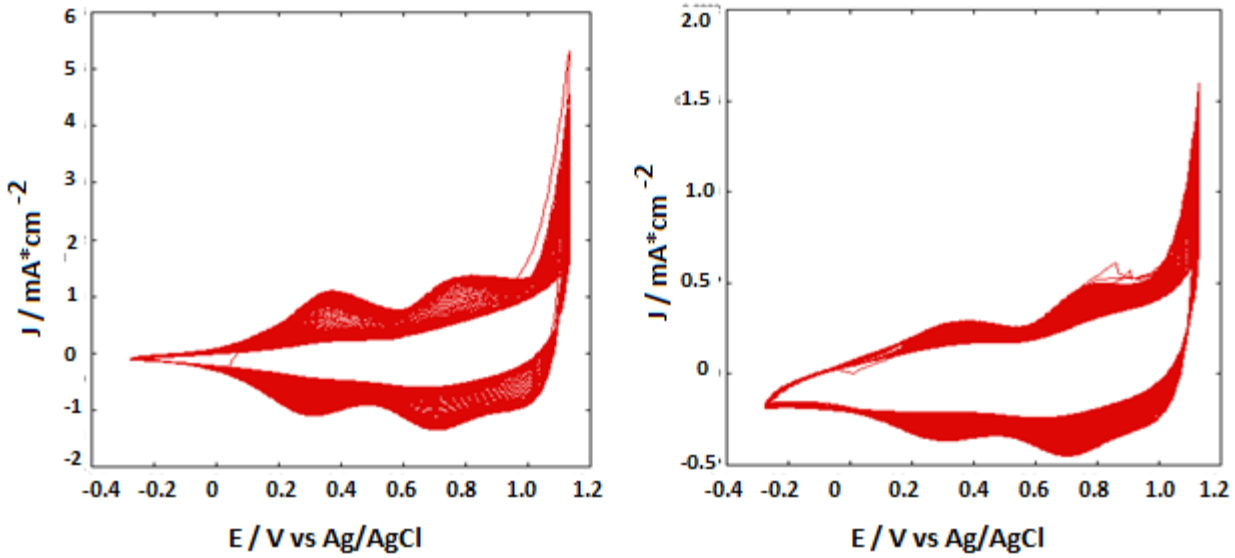

Figure 3. First eighty Voltametric cycles of two NiO films obtained via screen-printing. The electroactive electrode of NiO was cycled in the aqueous electrolyte 0.2 M KCl buffered by the acid/base couple $H_2PO_4^-/HPO_4^{2-}$. Scan rate: 5 mV s^{-1}. Left plot: l = 6 µm; right plot : l = 2 µm.

Figure 5 shows the comparison of the voltammograms generated by bare FTO and the electrochemically cycled film of screen-printed NiO within the potential range of NiO oxidation. The flatness of the voltammogram of cycled NiO indicates that the electroactivity of this electrochemically modified system is practically identical to the one of bare FTO. Such a finding supports the ascription of the observed phenomena to the occurrence of NiO electrochemical dissolution in aqueous electrolyte without employing the mass-sensitive technique of electrochemical quartz-crystal microbalance which requires the deposition of the electrodes on a substrate made of a proper piezoelectric crystal [88,89].

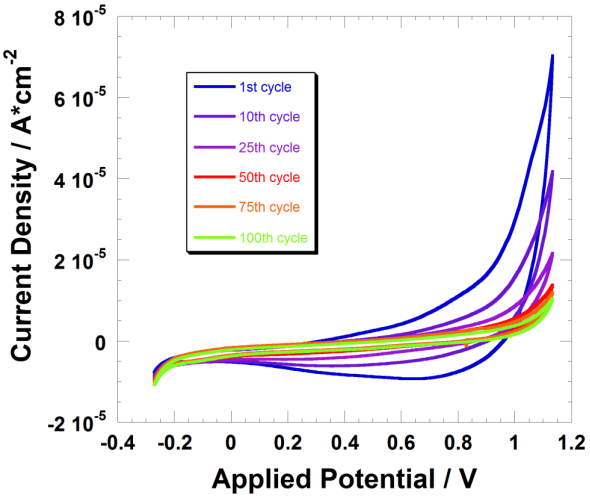

Figure 4. Selection of Voltametric cycles of a NiO thin film (l = 2 µm) obtained via screen-printing. The electroactive NiO was repetitively cycled in the aqueous electrolyte 0.2 M KCl buffered by the acid/base couple $H_2PO_4^-/HPO_4^{2-}$. Scan rate: 5 mV s^{-1}.

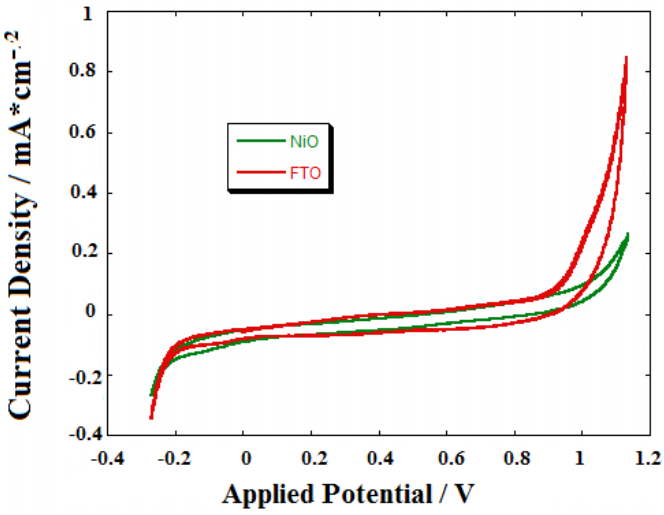

Figure 5. Comparison of the voltammograms recorded in the same electrolyte of Figure 4 when the working electrodes are bare FTO (red curve) and screen-printed NiO after 100 cycles (l = 2 µm, green curve). Voltametric responses were recorded at the scan rate of 5 mV s^{-1}.

As a further confirmation of the effect of electrochemical dissolution of NiO in aqueous electrolyte the optical transmission spectra of NiO in the pristine and electrochemically cycled version have been recorded (Figure 6). The comparison of

the transmittance curves clearly evidences an effect of thinning for NiO when it undergoes continuous electrochemical cycling in aqueous electrolyte (5 cycles).

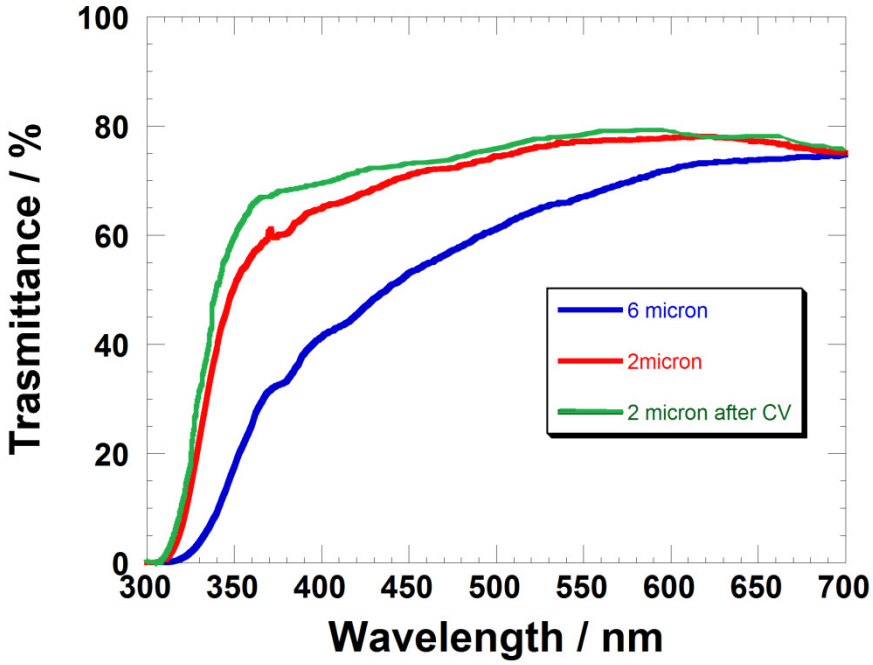

Figure 6. Comparison of the transmission spectra of NiO at two different thickness values (2 and 6 μm), prior and after the electrochemical cycling in aqueous electrolyte. It is evident a phenomenon of electrochemical dissolution of NiO in passing from pristine to the electrochemically cycled state with the latter having a smaller thickness with respect to the pristine version.

3.2 EIS analysis of screen-printed NiO electrodes

During EIS experiment the application of the potential of NiO oxidation does not provoke the dissolution of the NiO film since it has been observed that NiO gets dissolved in aqueous electrolyte upon repeated cycling but not after a single step of oxidation. We have effectuated a sampling of the electrochemical impedance spectra at seven different values of E_{appl} within the applied potential range $-0.2 \leq E_{appl} \leq 1.1$ V *vs* Ag/AgCl. The impedance spectra of the NiO films have been interpreted in terms of the equivalent circuit depicted in Figure 7[90]. The complete sets of

impedance data and the corresponding fitting curves are shown in Figures 8 and 9 when l = 2 and 6 μm, respectively. Data are presenting as both Nyquist and Bode plot (Figure 10, phase *vs* applied frequency). The latter is especially meaningful to evidence the change in the electric properties of the NiO film as a consequence of the polarization.

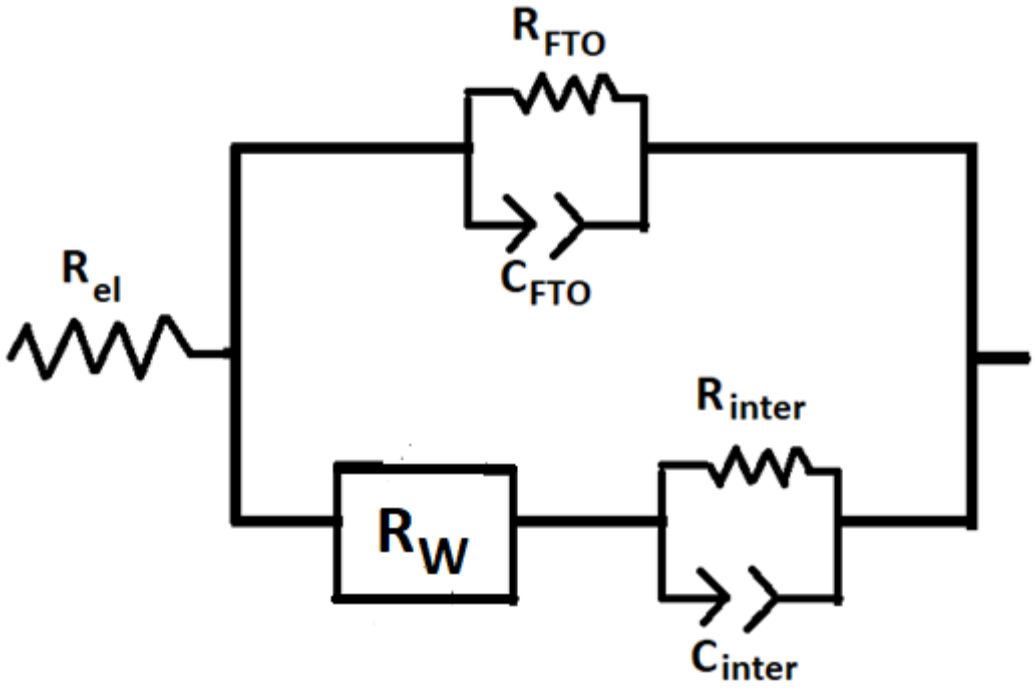

Figure 7. Equivalent circuit employed for the fit of the impedance spectra of screen-printed NiO (Figures 9 and 10).

In Figure 7, R_{el} represents the sum of the resistance of the electrolyte and the external contacts. This parameter is practically constant (i.e. 20 Ω) and does not vary with the variation of applied potential and film thickness. The terms C_{inter} (C_{FTO}) and R_{inter} (R_{FTO}) in Figure 7 refer to the electrical characteristics of the NiO/electrolyte (FTO/electrolyte) interface and indicate respectively the capacitance at the interface and the charge transfer resistance through the same interface. The NiO/electrolyte

interfacial charge transfer could be better described as a coupling between a hole in the NiO electrode and an anion coming from the aqueous solution (i.e. hydroxyl anions) as proved by XPS analyses[65]. Anyway, throughout the paper, we will refer to it as a charge transfer process. The FTO/electrolyte interface has been found to be exclusively meaningful for the thinner film. Upon increase of thickness the presence of voids diminishes gradually throughout the film of NiO as evidenced by the analysis of the voltammetries. This brings about a diminution of the chance of creating an extended FTO/electrolyte interface. Moreover, this term became negligible at lower applied potential, i.e. lower than 0.7V vs Ag/Ag^+ [90], as a consequence of the poor charging of the FTO layer[80]. The terms R_W is the Warburg resistance of the porous film and it should be directly proportional to the amount of stored charge in the NiO film under the different states of polarization. R_W refers to the charge transport/transfer properties of the NiO electrode, i.e. the ohmic resistance associated to the electrical transport through the NiO electrode. In the present case, the Warburg element refers to the diffusion of electronic carriers (i.e. the holes) coupled with counter-anions (i.e. hydroxyl anions) due to the aqueous environment and to the high porosity of the film.

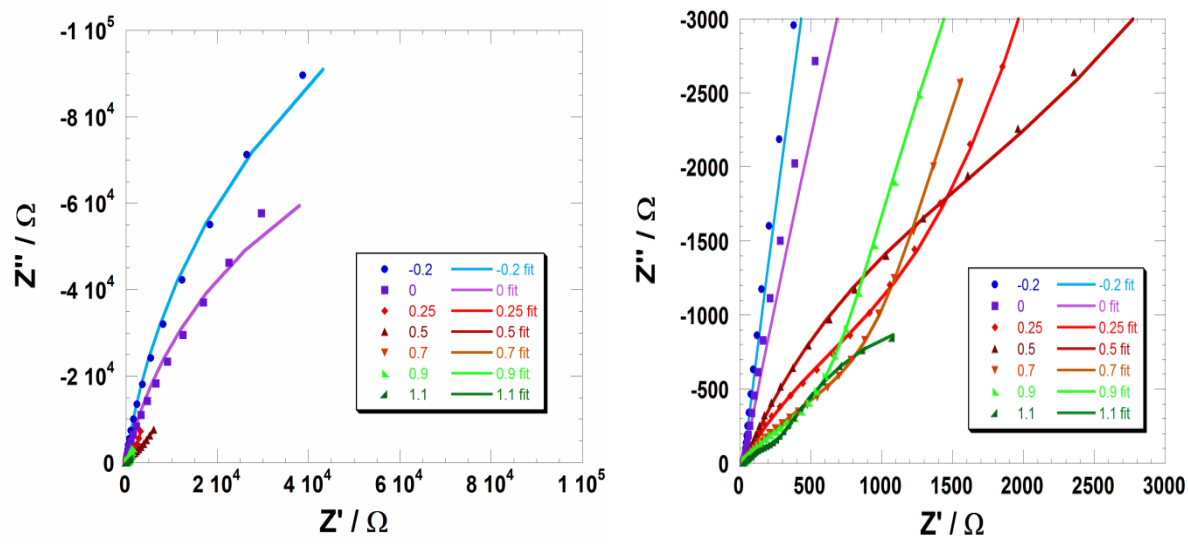

Figure 8. Nyquist plots of the electrochemical impedance spectra for the thinner screen-printed NiO electrode (l = 2 µm). Left: complete spectrum of impedance. Right: zoom of the impedance spectra in the range $0 \leq Z' \leq 3000$ Ω and $-3000 \leq Z'' \leq 0$ Ω. Spectra have been recorded at E_{appl} = -0.2, 0.0, 0.25, 0.5, 0.7 and 0.9 V *vs* Ag/AgCl. The continuous curves represent the fitting curves whereas the dots are the experimental points. Fits have been obtained with the equivalent circuit of Figure 7. The corresponding fitting parameters are shown in Table 3.

The pure capacitance element C_{inter} (Figure 7) is actually considered as a constant phase element (CPE), i.e. a term which allows an easier fit of the experimental data without influencing the reliability of the obtained parameters. The actual capacitance (C_{real}) could be calculated applying the following equation:

$$C_{real} = \frac{(C_{CPE} * R)^{\left(\frac{1}{n}\right)}}{R}$$

Where C_{CPE} and n are the two parameters constituting the CPE element and R is the value of the resistance associated to the latter. If n is equal to 1, the CPE acts a pure capacitive element. When the applied potential is lower than the NiO valence band edge, the electrode is expected to behave as an insulating film (R_W tends to infinite

values) and only the impedance features of the non-ohmic resistance of the NiO/aqueous electrolyte interface are observed.

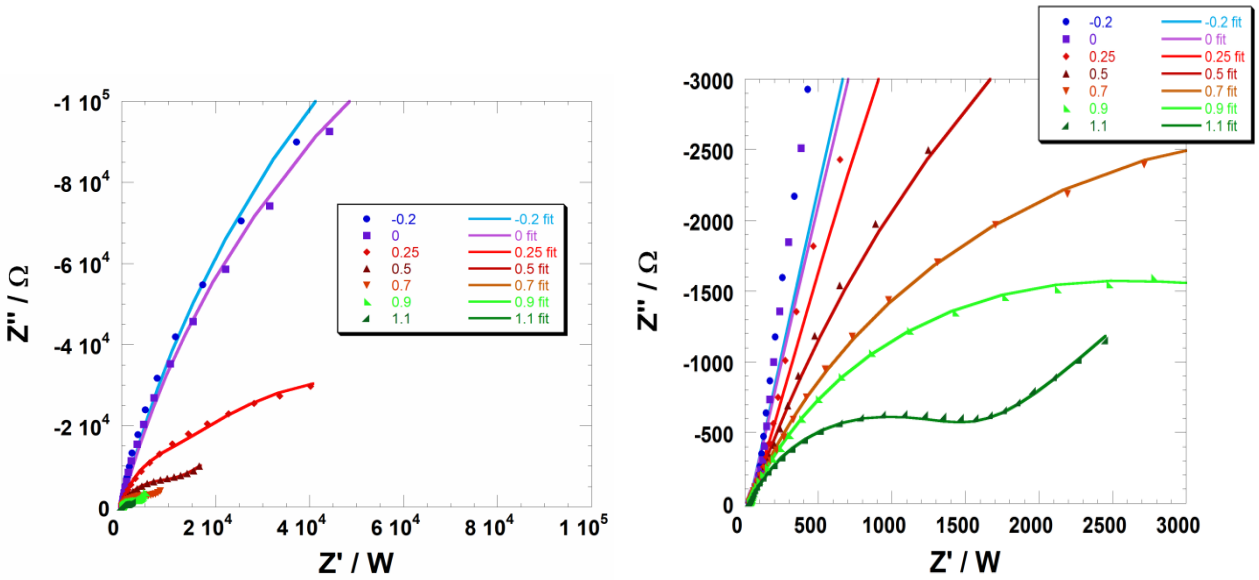

Figure 9. Nyquist plots of the electrochemical impedance spectra for the screen-printed NiO electrode (l = 6 µm). Left: complete spectrum of impedance. Right: zoom of the impedance spectra in the range $0 \leq Z' \leq 3000$ Ω and $-3000 \leq Z'' \leq 0$ Ω. Spectra have been recorded at E_{appl} = -0.2, 0.0, 0.25, 0.5, 0.7 and 0.9 V *vs* Ag/AgCl. The continuous curves represent the fitting curves whereas the dots are the experimental points. Fits have been obtained with the equivalent circuit of Figure 7. The corresponding fitting parameters are shown in Table 4.

Bode plots (Figure 10) display the dependence of the phase of the impedance on applied frequency. This way of representing the EIS data helps to clarify the kinetic features of the electrical transport through NiO. In particular, three different peaks could be distinguished in the EI spectra of the cell with the thinner NiO electrode whereas a thicker electrode generates only one broad peak upon increase of applied potential. The two additional peaks characteristic of the thinner electrode are ascribed to the process of charge transfer occurring at the FTO/electrolyte interface.

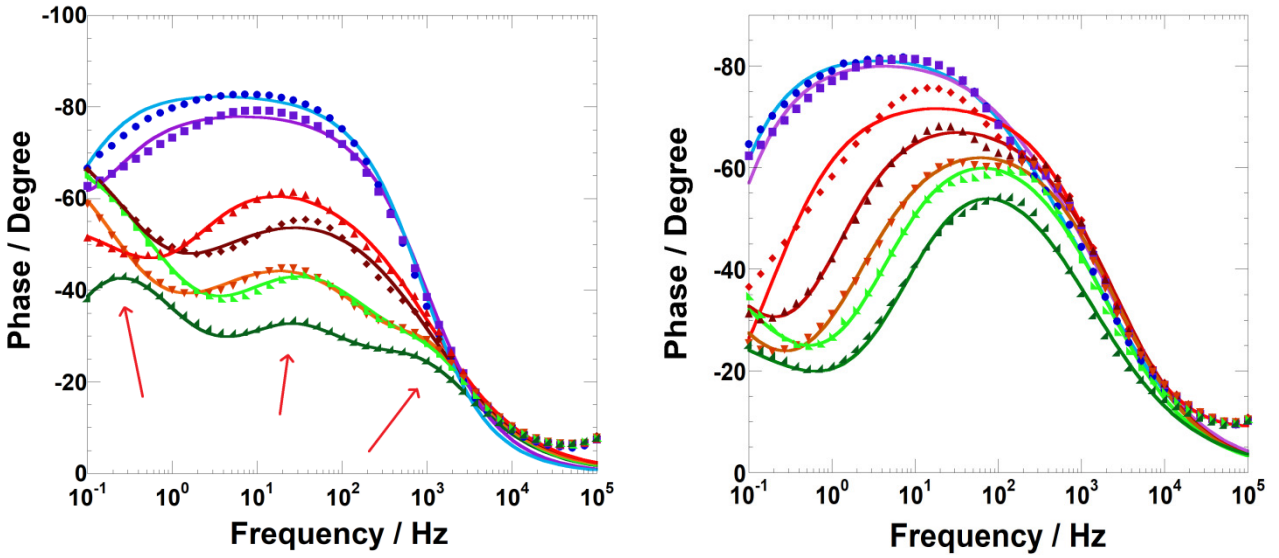

Figure 10. Bode plots of the cells with the (left) thinner and (right) thicker working electrode of NiO. In the left frame the three red arrows indicate the peaks in correspondence of which transitions between states with different transport properties take place.

The fitting values of the electrical elements constituting the equivalent circuit of Figure 7 are listed in Tables 3 and 4 when NiO working electrode was 2 and 6 μm thick, respectively. With regard to the thinner film of NiO (l = 2 μm), the values of R_{FTO} and C_{FTO} could be defined when the applied potential exceeds the threshold of 0.7 V *vs* Ag/AgCl (Table 1). When E_{appl} < 0.7 V *vs* Ag/AgCl the FTO/electrolyte is not relevant since the FTO layer is not sufficiently charged to start an event of charge transfer through its interface with the electrolyte. R_{FTO} and C_{FTO} vary in an opposite way with respect to E_{appl}, with R_{FTO}/C_{FTO} increasing/decreasing upon potential increase (Table 3). These findings would indicate that the FTO substrate does not behave exclusively as a polarisable electrode when NiO oxidation starts otherwise C_{FTO} would have been invariant.

E_{appl} / V *vs* Ag/AgCl	-0.20	0.00	0.25 V	0.50	0.70	0.90	1.10
R_{FTO} / Ω	-	-	-	-	12.7 ± 0.3	15.7 ± 0.2	33.6 ± 0.2
C_{FTO} / μF	-	-	-	-	64 ± 5	32 ± 3	14 ± 1
R_{inter} / Ω	106340 ± 4533	35182 ± 943	1848 ± 175	1693 ± 158	923 ±93	492 ±74	203 ±44
C_{inter} / μF	18 ± 3	23 ± 4	45 ± 6	56 ± 8	77 ± 15	87 ± 23	112 ± 25
R_W / kΩ	257 ± 1	135 ± 1	27.0 ± 0.8	12.6 ± 0.5	8.6 ± 0.4	7.2 ± 0.2	2.7 ± 0.1

Table 3. Fitting values of the variable electrical parameters relative to the EIS data of NiO electrode (l = 2 μm) at various values of applied potential. In the first row E_{appl} is expressed in V *vs* Ag/AgCl. The adopted model is the one depicted in Figure 7.

E_{appl} / V *vs* Ag/AgCl	-0.20	0.00	0.25	0.50	0.70	0.90	1.10
R_{inter} / Ω	146340 ± 7533	57136 ± 6123	25724 ± 2657	8548 ± 669	5580 ±397	3737 ±225	1238 ±84
C_{inter} / μF	21 ± 4	25 ± 3	97 ± 8	133 ± 12	174 ± 32	222 ± 21	240 ± 48
R_W/ kΩ	283 ± 1	144 ± 1	57.0 ± 2.8	27.6 ± 1.5	18.5 ± 1.2	14.8 ± 0.4	4.4 ± 0.3

Table 4. Fitting values of the variable electrical parameters relative to the EIS data of NiO electrode (l = 6 μm) at various values of applied potential. In the first row E_{appl} is expressed in V *vs* Ag/AgCl. The adopted model is the one depicted in Figure 7.

Moreover, the increase of R_{FTO} with the increase of E_{appl} (and the concomitant acceleration of NiO oxidation) indicates that FTO is involved in a process of charge transfer that is inhibited by the onset of the oxidation of NiO. At this concern we have considered the analysis of the electrochemical impedance spectra of bare FTO (Figure 11).

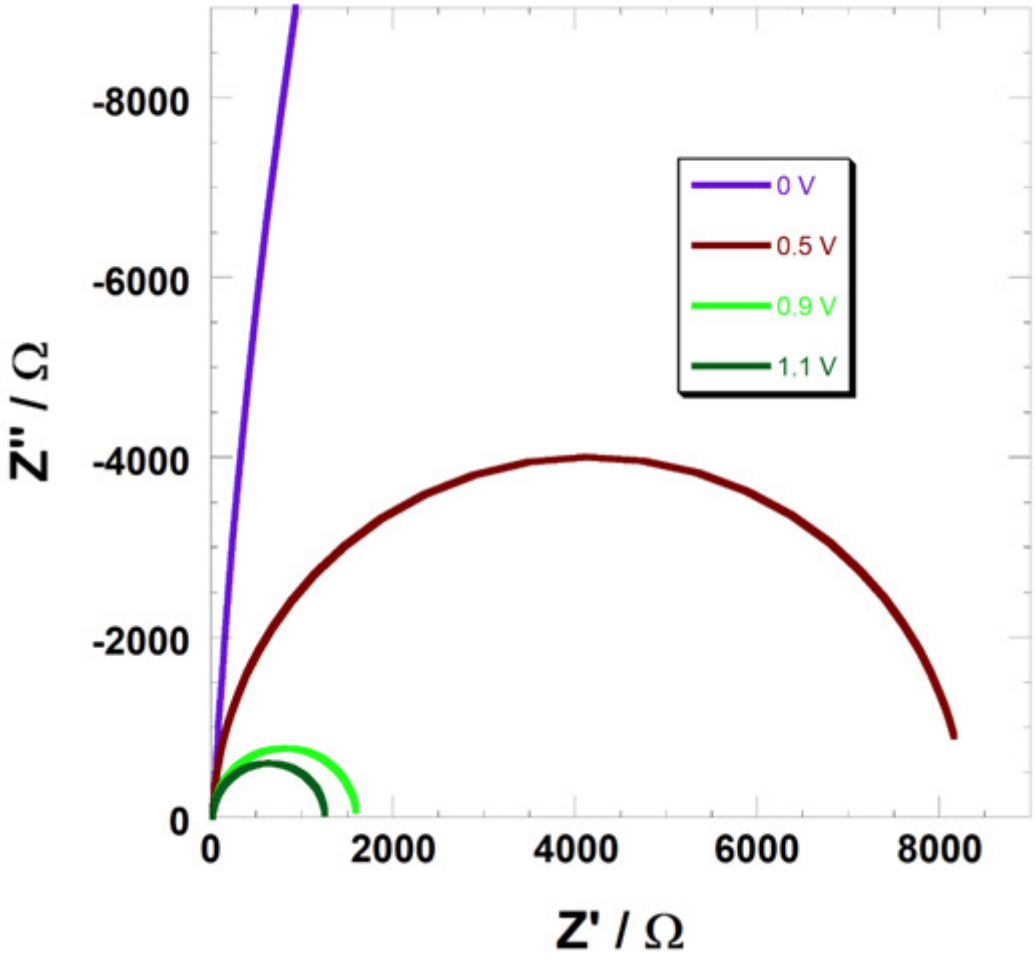

Figure 11. Nyquist plots of the electrochemical impedance spectra for bare FTO. when E_{appl} = 0.0, 0.5, 0.9 and 1.1 V *vs* Ag/AgCl.

Upon fitting of the experimental data in Figure 11 we found that the charge transfer resistance of bare FTO actually decreases with the applied potential being R_{FTO} =

1235, 1536, 8265 and 193324 Ω when E_{appl} is respectively 1.1, 0.9, 0.5 and 0.0 V *vs* Ag/AgCl. The trend of the interfacial capacitance is discordant with the one of R_{FTO} being C_{FTO} = 43, 40, 21 and 3 μF respectively for E_{appl} = 1.1, 0.9, 0.5 and 0.0 V *vs* Ag/AgCl. The charge transfer resistance of bare FTO is clearly larger than the one of NiO-coated FTO since NiO is known for having an electrocatalytic effect towards oxidative processes with respect to FTO[12].

As far as the resistive terms R_{inter} and R_W are concerned, both these terms decrease with the applied potential. This is consistent with the increase of the concentration of electronic and ionic charge carriers in the oxide film with the progress of oxidation on going from -0.2 to 1.1 V *vs* Ag/AgCl. Such a trend is common for both of NiO samples. The capacitive term C_{inter} depends directly on the amount of charge at the NiO/electrolyte surface. The observation of the increase of C_{inter} with E_{appl} is then largely expected. A very large increase of both R_W and R_{inter} is determined when the applied potential goes from 0.25 to 0 V *vs* Ag/AgCl. This is probably due to a change in the electronic nature of the NiO film: at applied potential lower than 0.25 V *vs* Ag/AgCl, the polarization superimposed on the electrode causes the filling of the surface-localized holes (onset of NiO reduction)[13,14] and the NiO film becomes more insulating upon the neutralization of these defective sites localized on NiO surface. As previously stated, R_W is mainly controlled by the amount of stored charge in the electrode and a decrease of the stored charge is associated with a lower value of R_W. The transition from a semiconducting state to an insulating one is not sharp and for the attainment of an insulating state of NiO more negative potential values need to

445 be applied. On the other hand, in aqueous environment the molecular hydrogen
446 evolution reaction takes place at applied potential lower than -0.2 V *vs* Ag/AgCl ad
447 prevents the attainment of insulating NiO upon electrochemical polarization.
448 Anyway, the transition semiconductor/insulator is somewhat supported by the
449 remarkable decrease of the interfacial capacitance of the film upon diminution of the
450 applied potential (Tables 3 and 4). The fitting parameters have a common trend with
451 E_{appl} for both values of NiO film thickness. The thicker film results more resistive
452 than the thinner. This is somewhat unexpected since an increase of electrode
453 thickness should lead to a larger exposed surface and a higher amount of charge
454 exchanged by the oxidized electrode when the electrode is homogeneously
455 mesoporous throughout the whole thickness. It has been previously observed that
456 screen-printed NiO electrodes are not homogeneously porous if the thickness exceeds
457 3-4 μm[87] A 6 μm-thick film of screen-printed is expected to be a sequence of layers
458 differing in porosity with the layers of more open morphology located nearer the FTO
459 substrate and the more compact layers positioned at the interface with the electrolyte.
460 This lack of homogeneity would explain also the decrease of the volume density of
461 the charge exchanged by the NiO electrode in passing from the thinner to the thicker
462 film (*vide supra*). The FE-SEM image of the cross-section of the thicker film of NiO
463 (Figure 12) reveals that the electrode is formed by the superposition of an upper
464 compact layer (with thickness of about 2.5 μm) and a porous (and thicker) layer with
465 approximate thickness of ~ 3.9 μm.
466

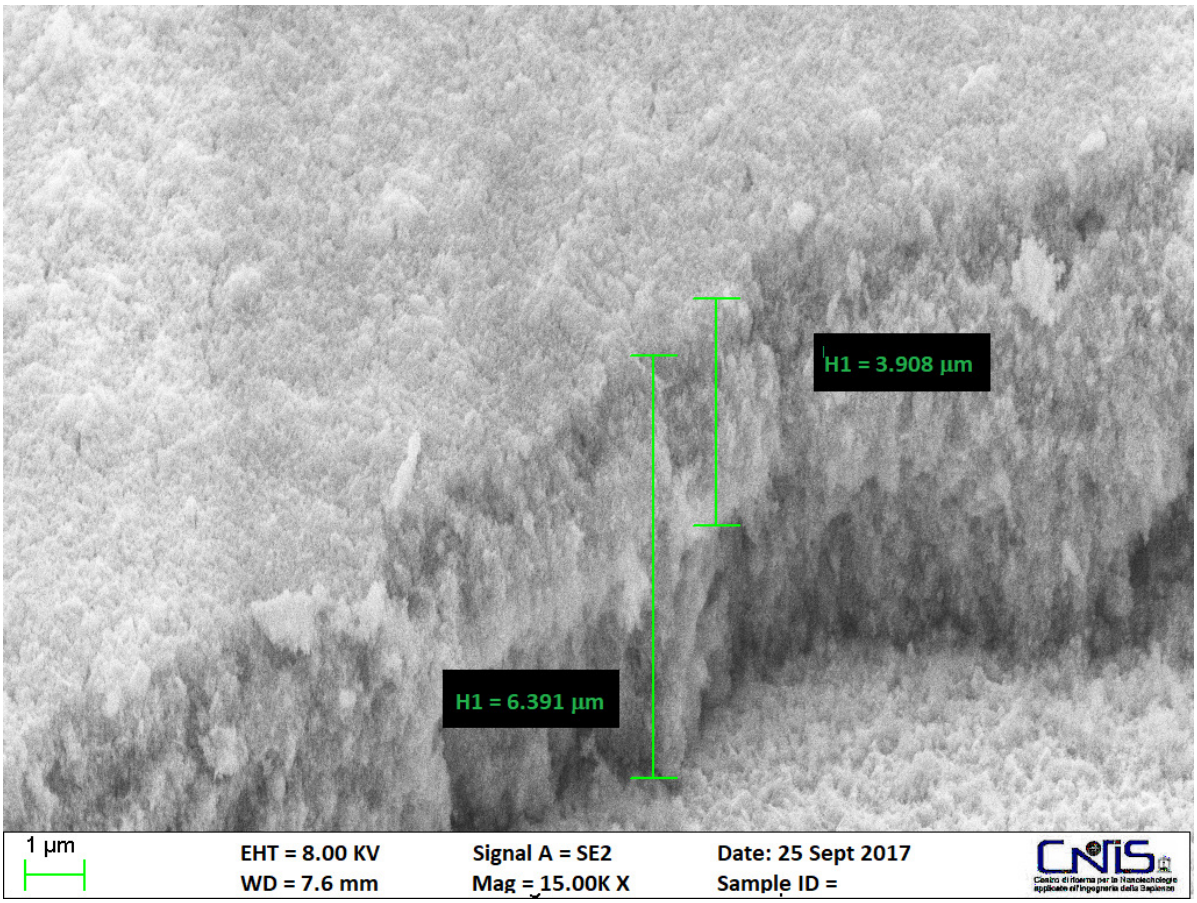

Figure 12. FE-SEM image of the cross section of screen-printed NiO electrode (l = 6µm).

The observation of such a morphology justifies the higher resistivity of the thicker film with respect to the thinner. In an aqueous environment, the holes that traverse the NiO film are coupled with the hydroxyl anions with consequent formation of a system with mixed conduction[91]. Such a mechanism retains its validity regardless of film thickness. If the film possesses variable morphology with porous layers adjacent to more compact layers, the flow of the charge carriers in the mixed conduction regime will results more hindered in correspondence of the compact layers. A uniformly porous film of oxidized NiO can drain the charge-compensating hydroxide anions (in case of an aqueous electrolyte) externally on its surface

480 throughout the whole layer of NiO due to the electric field of the holes which move
481 within oxidized NiO. In presence of a compact layer of NiO the charge compensating
482 anions cannot move along the NiO/electrolyte interface through the whole thickness
483 of the film. As a consequence of this physical limitation, the thicker film of NiO with
484 compact features displays a larger electrical resistance with respect to the thinner
485 film. When $E_{appl} < 0$ V *vs* Ag/AgCl, NiO behaves as an insulating material and in this
486 case the electrical properties of charge transport are practically insensitive to the
487 differences in morphology. The thinner film is then as resistive as the thicker one and
488 the characteristic of NiO morphology becomes crucial exclusively when NiO has to
489 sustain a current, i.e. in the semiconducting state for $E_{appl} > 0.1$ V *vs* Ag/AgCl.
490 From the comparison of the values in Tables 3 and 4 it results that R_{inter} is generally
491 higher for the thicker film. This is a consequence of the presence of a more extended
492 portion of compact layer in the thicker electrode with respect to thinner one. There is
493 a correlation between R_{inter} and R_W since a high value of R_{inter} provokes charge
494 accumulation on electrode surface that renders harder the further charge transport
495 through the interface and successively through the NiO film. This hypothesis is
496 supported by the generally higher values of C_{inter} for the thicker electrode with respect
497 to the thinner electrode for any value of NiO polarization within the range of
498 potential here examined. Again, the electrical parameters tend to assume the same
499 values for the NiO films differing in thickness (and morphology) when null or
500 negative values of potential are applied and charge transport phenomena are
501 inhibited.

4. Conclusions

Nanostructured NiO electrodes in the configuration of thin films (l < 7 μm) were prepared via screen-printing of precursor paste and the electrochemical properties were studied in aqueous solution. In this electrolytic ambient NiO manifests two reversible processes of solid state oxidation within the potential range 0.1 - 1.0 V *vs* Ag/AgCl. The kinetics of these electrochemical processes resulted controlled by a step confined on the electrode surface. Continuous electrochemical cycling brings about the dissolution of these nanoporous NiO films as verified by the progressive decrease of the current exchanged by NiO upon cycling and by the decrease of optical absorption of the film on going from the pristine to the electrochemically cycled state. The electrochemical oxidation brings about a general diminution of the intrinsic electrical resistance of screen-printed NiO as revealed by the analysis of the electrochemical impedance spectra. The combined analysis of the morphological characteristics and of the impedance spectra of NiO electrodes has shown that screen-printed electrodes present a non homogeneous porosity when NiO films are thicker than 4 μm. NiO film thickening brings about an increase of film compactness (or decrease of porosity). Such a morphological feature of the thicker films is accompanied by larger values of both resistive terms (interfacial and bulk) and double layer capacitance with respect to the thinner film with l < 3 μm. In particular, the 2 μm thick film of NiO obtained via screen-printing is porous throughout the whole thickness and does not cover uniformly the FTO substrate. The last conclusion

has been drawn for the necessary inclusion of the electrical features of the FTO/electrolyte interface for the simulation of the electrochemical impedance spectra of thinner NiO films.

Acknowledgments

Authors acknowledge the financial support of Ateneo Sapienza (protocol no: 2011/VG1-C26A11PKS2). Authors wish also to thank Prof. Ruggero Caminiti (Director of CNIS - Centro di Ricerca per le Nanotecnologie Applicate all'Ingegneria, an interdepartmental centre of the University of Rome LA SAPIENZA) and Dr. Francesco Mura (CNIS), for the realization of the SEM images presented in this paper. CNIS is gratefully acknowledged for having sponsored the realization of these images.

References

[1] S.M. Wilhelm, Photoelectrochemical Characterization of the Passive Films on Iron and Nickel, J. Electrochem. Soc. 128 (1981) 1668–1674. doi:10.1149/1.2127708.

[2] S. Passerini, B. Scrosati, Characterization of Nonstoichiometric Nickel Oxide Thin-Film Electrodes, J. Electrochem. Soc. 141 (1994) 889–895. doi:10.1149/1.2054853.

[3] R.W. Wright, J.P. Andrews, Temperature Variation of the Electrical Properties of Nickel Oxide, Proc. Phys. Soc. Sect. A. 62 (1949) 446–455. doi:10.1088/0370-1298/62/7/306.

[4] S.P. Mitoff, Electrical conductivity and thermodynamic equilibrium in nickel oxide, J. Chem. Phys. 727 (1961) 882–889. doi:10.1063/1.1701231.

[5] M.W. Vernon, M.C. Lovell, Anomalies in the electrical conductivity of nickel oxide above room temperature, J. Phys. Chem. Solids. 27 (1966) 1125–1131. doi:10.1016/0022-3697(66)90087-4.

[6] R. Farhi, G. Petot-Ervas, Electrical conductivity and chemical diffusion coefficient measurements in single crystalline nickel oxide at high temperatures, Solid State Commun. 26 (1978) 1169–1173. doi:10.1016/0038-1098(78)91288-7.

[7] M. Nachman, L.N. Cojocaru, L. V. Ribco, Electrical Properties of Non-Stoichiometric Nickel Oxide, Phys. Status Solidi. 8 (1965) 773–783. doi:10.1002/pssb.19650080316.

[8] F.J. Morin, Electrical properties of α-Fe2O3, Phys. Rev. 93 (1954) 1195–1199.

556 doi:10.1103/PhysRev.93.1195.
557 [9] I. Popescu, E. Heracleous, Z. Skoufa, A.A. Lemonidou, I.-C. Marcu, Study by electrical
558 conductivity measurements of semiconductive and redox properties of M-doped NiO (
559 M=Li,Mg,Al,Ga,Ti,Nb) catalysts for the oxidative dehydrogenation of ethane, Phys. Chem.
560 Chem. Phys. 16 (2014) 4962–4970. doi:10.1039/c3cp54817a.
561 [10] S.R. Morrison, Electrochemistry at Semiconductor and Oxidized Metal Electrodes, Plenum
562 Press, New York, 1980.
563 [11] A. Nattestad, M. Ferguson, R. Kerr, Y.-B. Cheng, U. Bach, Dye-sensitized nickel(II)oxide
564 photocathodes for tandem solar cell applications., Nanotechnology. 19 (2008) 295304.
565 doi:10.1088/0957-4484/19/29/295304.
566 [12] S. Sheehan, G. Naponiello, F. Odobel, D.P. Dowling, A. Di Carlo, D. Dini, Comparison of
567 the photoelectrochemical properties of RDS NiO thin films for p-type DSCs with different
568 organic and organometallic dye-sensitizers and evidence of a direct correlation between cell
569 efficiency and charge recombination, J. Solid State Electrochem. 19 (2015) 975–986.
570 doi:10.1007/s10008-014-2703-9.
571 [13] M. Awais, D. Dini, J.M. Don MacElroy, Y. Halpin, J.G. Vos, D.P. Dowling, Electrochemical
572 characterization of NiO electrodes deposited via a scalable powder microblasting technique,
573 J. Electroanal. Chem. 689 (2013) 185–192. doi:10.1016/j.jelechem.2012.11.025.
574 [14] M. Awais, D.D. Dowling, M. Rahman, J.G. Vos, F. Decker, D. Dini, Spray-deposited NiO x
575 films on ITO substrates as photoactive electrodes for p-type dye-sensitized solar cells, in: J.
576 Appl. Electrochem., 2013: pp. 191–197. doi:10.1007/s10800-012-0506-1.
577 [15] G. Naponiello, I. Venditti, V. Zardetto, D. Saccone, A. Di Carlo, I. Fratoddi, C. Barolo, D.
578 Dini, Photoelectrochemical characterization of squaraine-sensitized nickel oxide cathodes
579 deposited via screen-printing for p-type dye-sensitized solar cells, Appl. Surf. Sci. 356 (2015)
580 911–920. doi:10.1016/j.apsusc.2015.08.171.
581 [16] M. Bonomo, G. Naponiello, D.C. A, D. Dini, Characterization of Screen-Printed Nickel
582 Oxide Electrodes for p -type Dye- Sensitized Solar Cells, J Mater Sci Nanotechnol. 4 (2016)
583 201. doi:10.15744/2348-9812.4.201.
584 [17] M. Bonomo, G. Naponiello, I. Venditti, V. Zardetto, A. Di Carlo, D. Dini, Electrochemical
585 and Photoelectrochemical Properties of Screen-Printed Nickel Oxide Thin Films Obtained
586 from Precursor Pastes with Different Compositions, J. Electrochem. Soc. 164 (2017) H137–
587 H147. doi:10.1149/2.0051704jes.
588 [18] L. Lepleux, B. Chavillon, Y. Pellegrini, E. Blart, L. Cario, S. Jobic, F. Odobel, Simple and
589 reproducible procedure to prepare self-nanostructured NiO films for the fabrication of P-type
590 dye-sensitized solar cells, Inorg. Chem. 48 (2009) 8245–8250. doi:10.1021/ic900866g.
591 [19] A. Renaud, B. Chavillon, L. Cario, L. Le Pleux, N. Szuwarski, Y. Pellegrin, E. Blart, E.
592 Gautron, F. Odobel, S. Jobic, Origin of the black color of NiO used as photocathode in p-
593 type dye-sensitized solar cells, J. Phys. Chem. C. 117 (2013) 22478–22483.
594 doi:10.1021/jp4055457.
595 [20] M.M. Sk, C.Y. Yue, K. Ghosh, R.K. Jena, Review on advances in porous nanostructured
596 nickel oxides and their composite electrodes for high-performance supercapacitors, J. Power
597 Sources. 308 (2016) 121–140. doi:10.1016/j.jpowsour.2016.01.056.
598 [21] S. Chu, K. Gerasopoulos, R. Ghodssi, Tobacco mosaic virus-templated hierarchical Ni/NiO
599 with high electrochemical charge storage performances, Electrochim. Acta. 220 (2016) 184–
600 192. doi:10.1016/j.electacta.2016.10.106.
601 [22] F. Lin, H. Wang, G. Wang, Facile Synthesis of Hollow Polyhedral (Cubic, Octahedral and
602 Dodecahedral) NiO with Enhanced Lithium Storage Capabilities, Electrochim. Acta. 211
603 (2016) 207–216. doi:10.1016/j.electacta.2016.05.195.
604 [23] S. Passerini, B. Scrosati, Electrochromism of thin-film nickel oxide electrodes, Solid State
605 Ionics. 53–56 (1992) 520–524. doi:10.1016/0167-2738(92)90423-M.
606 [24] F. Decker, The electrochromic process in non-soichiometric nickel oxide thin film electrodes,

Electrochim. Acta. 37 (1992) 1033–1038. doi:http://dx.doi.org/10.1016/0013-4686(92)85220-F.
[25] G. Cai, X. Wang, M. Cui, P. Darmawan, J. Wang, A.L.S. Eh, P.S. Lee, Electrochromo-supercapacitor based on direct growth of NiO nanoparticles, Nano Energy. 12 (2015) 258–267. doi:10.1016/j.nanoen.2014.12.031.
[26] R.T. Wen, C.G. Granqvist, G.A. Niklasson, Anodic electrochromism for energy-efficient windows: Cation/anion-based surface processes and effects of crystal facets in nickel oxide thin films, Adv. Funct. Mater. 25 (2015) 3359–3370. doi:10.1002/adfm.201500676.
[27] M. Da Rocha, A. Rougier, Electrochromism of non-stoichiometric NiO thin film: as single layer and in full device, Appl. Phys. A Mater. Sci. Process. 122 (2016). doi:10.1007/s00339-016-9923-z.
[28] A.I. Inamdar, A.C. Sonavane, S.M. Pawar, Y. Kim, J.H. Kim, P.S. Patil, W. Jung, H. Im, D.Y. Kim, H. Kim, Electrochromic and electrochemical properties of amorphous porous nickel hydroxide thin films, Appl. Surf. Sci. 257 (2011) 9606–9611. doi:10.1016/j.apsusc.2011.06.079.
[29] R.T. Wen, C.G. Granqvist, G.A. Niklasson, Anodic Electrochromic Nickel Oxide Thin Films: Decay of Charge Density upon Extensive Electrochemical Cycling, ChemElectroChem. 3 (2016) 266–275. doi:10.1002/celc.201500457.
[30] Y. Chen, Y. Wang, P. Sun, P. Yang, L. Du, W. Mai, Nickel oxide nanoflake-based bifunctional glass electrodes with superior cyclic stability for energy storage and electrochromic applications, J. Mater. Chem. A. 3 (2015) 20614–20618. doi:10.1039/c5ta04011f.
[31] C.C. Zhao, C. Chen, F.L. Du, J.M. Wang, Template synthesis of NiO ultrathin nanosheets using polystyrene nanospheres and their electrochromic properties, Rsc Adv. 5 (2015) 38533–38537. doi:10.1039/c5ra04571a.
[32] J. Denayer, G. Bister, P. Simonis, P. Colson, A. Maho, P. Aubry, B. Vertruyen, C. Henrist, V. Lardot, F. Cambier, R. Cloots, Surfactant-assisted ultrasonic spray pyrolysis of nickel oxide and lithium-doped nickel oxide thin films, toward electrochromic applications, Appl. Surf. Sci. 321 (2014) 61–69. doi:10.1016/j.apsusc.2014.09.128.
[33] H. Moulki, C. Faure, M. Mihelčič, A. Šurca Vuk, F. Švegl, B. Orel, G. Campet, M. Alfredsson, A. V. Chadwick, D. Gianolio, A. Rougier, Electrochromic performances of nonstoichiometric NiO thin films, in: Thin Solid Films, 2014: pp. 63–66. doi:10.1016/j.tsf.2013.10.154.
[34] D. Dini, Y. Halpin, J.G. Vos, E.A. Gibson, The influence of the preparation method of NiO<inf>x</inf> photocathodes on the efficiency of p-type dye-sensitized solar cells, Coord. Chem. Rev. 304–305 (2015) 179–201. doi:10.1016/j.ccr.2015.03.020.
[35] A. Nattestad, I. Perera, L. Spiccia, Developments in and prospects for photocathodic and tandem dye-sensitized solar cells, J. Photochem. Photobiol. C Photochem. Rev. 28 (2016) 44–71. doi:10.1016/j.jphotochemrev.2016.06.003.
[36] S. Yun, Y. Qin, A.R. Uhl, N. Vlachopoulos, M. Yin, D.D. Li, X. Han, A. Hagfeldt, New-Generation Integrated Devices based on Dye-Sensitized and Perovskite Solar Cells, Energy Environ. Sci. (2018). doi:10.1039/C7EE03165C.
[37] G. Li, Y. Jiang, S. Deng, A. Tam, P. Xu, M. Wong, H.S. Kwok, Overcoming the Limitations of Sputtered Nickel Oxide for High-Efficiency and Large-Area Perovskite Solar Cells, Adv. Sci. 4 (2017). doi:10.1002/advs.201700463.
[38] S. Passerini, J. Scarminio, B. Scrosati, D. Zane, F. Decker, Thin metal oxide films on transparent substrates for Li-insertion devices, J. Appl. Electrochem. 23 (1993) 1187–1195. doi:10.1007/BF00625594.
[39] M. Bonomo, A.G. Marrani, V. Novelli, M. Awais, D.P. Dowling, J.G. Vos, D. Dini, Surface properties of nanostructured NiO undergoing electrochemical oxidation in 3-methoxy-propionitrile, Appl. Surf. Sci. 403 (2017) 441–447. doi:10.1016/j.apsusc.2017.01.202.

[40] G. Boschloo, A. Hagfeldt, Spectroelectrochemistry of nanostructured NiO, J. Phys. Chem. B. 105 (2001) 3039–3044. doi:10.1021/jp003499s.
[41] N. Li, E.A. Gibson, P. Qin, G. Boschloo, M. Gorlov, A. Hagfeldt, L. Sun, Dou ble-layered NiO photocathodes for p-Type DSSCs with record IPCE, Adv. Mater. 22 (2010) 1759–1762. doi:10.1002/adma.200903151.
[42] M. Awais, M. Rahman, J.M. Don MacElroy, N. Coburn, D. Dini, J.G. Vos, D.P. Dowling, Deposition and characterization of NiOx coatings by magnetron sputtering for application in dye-sensitized solar cells, Surf. Coatings Technol. 204 (2010) 2729–2736. doi:10.1016/j.surfcoat.2010.02.027.
[43] M. Awais, M. Rahman, J.M. Don MacElroy, D. Dini, J.G. Vos, D.P. Dowling, Application of a novel microwave plasma treatment for the sintering of nickel oxide coatings for use in dye-sensitized solar cells, Surf. Coatings Technol. 205 (2011) S245–S249. doi:10.1016/j.surfcoat.2011.01.020.
[44] X.L. Zhang, F. Huang, A. Nattestad, K. Wang, D. Fu, A. Mishra, P. Bäuerle, U. Bach, Y.-B. Cheng, Enhanced open-circuit voltage of p-type DSC with highly crystalline NiO nanoparticles., Chem. Commun. (Camb). 47 (2011) 4808–10. doi:10.1039/c0cc05445c.
[45] S. Powar, Q. Wu, M. Weidelener, A. Nattestad, Z. Hu, A. Mishra, P. Bauerle, L. Spiccia, Y.-B. Cheng, U. Bach, Improved photocurrents for p-type dye-sensitized solar cells using nano-structured nickel(ii) oxide microballs, Energy Environ. Sci. 5 (2012) 8896–8900. doi:10.1039/C2EE22127F.
[46] A.A. Yadav, U.J. Chavan, Influence of substrate temperature on electrochemical supercapacitive performance of spray deposited nickel oxide thin films, J. Electroanal. Chem. 782 (2016) 36–42. doi:10.1016/j.jelechem.2016.10.006.
[47] S.A. Abbas, K.D. Jung, Preparation of mesoporous microspheres of NiO with high surface area and analysis on their pseudocapacitive behavior, Electrochim. Acta. 193 (2016) 145–153. doi:10.1016/j.electacta.2016.02.054.
[48] J. Zhao, H. Liu, Q. Zhang, Preparation of NiO nanoflakes under different calcination temperatures and their supercapacitive and optical properties, Appl. Surf. Sci. 392 (2017) 1097–1106. doi:10.1016/j.apsusc.2016.09.128.
[49] M. Bonomo, N. Barbero, F. Matteocci, A. Di Carlo, C. Barolo, D. Dini, Beneficial Effect of Electron-Withdrawing Groups on the Sensitizing Action of Squaraines for p-Type Dye-Sensitized Solar Cells, J. Phys. Chem. C. 120 (2016) 16340–16353. doi:10.1021/acs.jpcc.6b03965.
[50] M. Awais, D.P. Dowling, F. Decker, D. Dini, Electrochemical characterization of nanoporous nickel oxide thin films spray-deposited onto indium-doped tin oxide for solar conversion scopes, Adv. Condens. Matter Phys. 2015 (2015) 186375. doi:10.1155/2015/186375.
[51] M. Awais, D.D. Dowling, F. Decker, D. Dini, Photoelectrochemical properties of mesoporous NiO x deposited on technical FTO via nanopowder sintering in conventional and plasma atmospheres, Springerplus. 4 (2015) 564. doi:10.1186/s40064-015-1265-3.
[52] M. Awais, E. Gibson, J.G. Vos, D.P. Dowling, A. Hagfeldt, D. Dini, Fabrication of Efficient NiO Photocathodes Prepared via RDS with Novel Routes of Substrate Processing for p-Type Dye-Sensitized Solar Cells, ChemElectroChem. 1 (2014) 384. doi:10.1002/celc.201300178.
[53] M.K. Brennaman, R.J. Dillon, L. Alibabaei, M.K. Gish, C.J. Dares, D.L. Ashford, R.L. House, G.J. Meyer, J.M. Papanikolas, T.J. Meyer, Finding the Way to Solar Fuels with Dye-Sensitized Photoelectrosynthesis Cells, J. Am. Chem. Soc. 138 (2016) 13085. doi:10.1021/jacs.6b06466.
[54] D.A. Hoogeveen, M. Fournier, S.A. Bonke, A. Nattestad, A. Mishra, P. Bäuerle, L. Spiccia, A.J. Mozer, A.N. Simonov, Origin of Photoelectrochemical Generation of Dihydrogen by a Dye-Sensitized Photocathode without an Intentionally Introduced Catalyst, J. Phys. Chem. C. 121 (2017) 25836–25846. doi:10.1021/acs.jpcc.7b08067.

[55] D. Wang, M. V Sheridan, B. Shan, B.H. Farnum, S.L. Marquard, B.D. Sherman, M.S. Eberhart, A. Nayak, C.J. Dares, A.K. Das, R.M. Bullock, T.J. Meyer, Layer-by-Layer Molecular Assemblies for Dye-Sensitized Photoelectrosynthesis Cells Prepared by Atomic Layer Deposition, J. Am. Chem. Soc. 139 (2017) 14518–14525. doi:10.1021/jacs.7b07216.
[56] B.D. Sherman, M. V. Sheridan, K.R. Wee, S.L. Marquard, D. Wang, L. Alibabaei, D.L. Ashford, T.J. Meyer, A Dye-Sensitized Photoelectrochemical Tandem Cell for Light Driven Hydrogen Production from Water, J. Am. Chem. Soc. 138 (2016) 16745–16753. doi:10.1021/jacs.6b10699.
[57] I. Concina, Z.H. Ibupoto, A. Vomiero, Semiconducting Metal Oxide Nanostructures for Water Splitting and Photovoltaics, Adv. Energy Mater. 139 (2017) 1700706. doi:10.1002/aenm.201700706.
[58] M.D. Brady, R.N. Sampaio, D. Wang, T.J. Meyer, G.J. Meyer, Dye-Sensitized Hydrobromic Acid Splitting for Hydrogen Solar Fuel Production, J. Am. Chem. Soc. 139 (2017) 15612–15615. doi:10.1021/jacs.7b09367.
[59] F. Bella, C. Gerbaldi, C. Barolo, M. Grätzel, Aqueous dye-sensitized solar cells, Chem. Soc. Rev. 44 (2015) 3431–3473. doi:10.1039/C4CS00456F.
[60] F. Bella, S. Galliano, M. Falco, G. Viscardi, C. Barolo, M. Grätzel, C. Gerbaldi, Unveiling iodine-based electrolytes chemistry in aqueous dye-sensitized solar cells, Chem. Sci. 7 (2016) 4480–4490. doi:10.1039/C6SC01145D.
[61] H. Liu, W. Xiang, H. Tao, Probing the influence of lithium cation as electrolyte additive for the improved performance of p-type aqueous dye sensitized solar cells, J. Photochem. Photobiol. A Chem. 344 (2017) 199–205. doi:10.1016/j.jphotochem.2017.05.019.
[62] W. Xiang, D. Chen, R.A. Caruso, Y.B. Cheng, U. Bach, L. Spiccia, The effect of the scattering layer in dye-sensitized solar cells employing a cobalt-based aqueous gel electrolyte, ChemSusChem. 8 (2015) 3704–3711. doi:10.1002/cssc.201500627.
[63] C.T. Li, R.Y.Y. Lin, J.T. Lin, Sensitizers for aqueous-based solar cells, Chem. - An Asian J. 12 (2017) 486–496. doi:10.1002/asia.201601627.
[64] V. Novelli, M. Awais, D.P. Dowling, D. Dini, Electrochemical Characterization of Rapid Discharge Sintering (RDS) NiO Cathodes for Dye-Sensitized Solar Cells of p-Type, Am. J. Anal. Chem. 6 (2015) 176–187. doi:10.4236/ajac.2015.62016.
[65] A.G. Marrani, V. Novelli, S. Sheehan, D.P. Dowling, D. Dini, Probing the redox states at the surface of electroactive nanoporous nio thin films, ACS Appl. Mater. Interfaces. 6 (2014) 143–152. doi:10.1021/am403671h.
[66] A. Tarola, D. Dini, E. Salatelli, F. Andreani, F. Decker, Electrochemical impedance spectroscopy of polyalkylterthiophenes, Electrochim. Acta. 44 (1999) 4189–4193.
[67] M.E. Orazem, B. Tribollet, Electrochemical Impedance Spectroscopy, 2008. doi:10.1002/9780470381588.
[68] A. Sacco, Electrochemical impedance spectroscopy: Fundamentals and application in dye-sensitized solar cells, Renew. Sustain. Energy Rev. 79 (2017) 814–829. doi:10.1016/j.rser.2017.05.159.
[69] M.E.G. Lyons, R.L. Doyle, I. Godwin, M. O'Brien, L. Russell, Hydrous Nickel Oxide: Redox Switching and the Oxygen Evolution Reaction in Aqueous Alkaline Solution, J. Electrochem. Soc. 159 (2012) H932–H944. doi:10.1149/2.078212jes.
[70] M.A. Sattar, B.E. Conway, Electrochemistry of the nickel-oxide electrode-VI. Surface oxidation of nickel anodes in alkaline solution, Electrochim. Acta. 14 (1969) 695–710. doi:10.1016/0013-4686(69)80025-3.
[71] D. Yohe, A. Riga, R. Greef, E. Yeager, Electrochemical properties of nickel oxide, Electrochim. Acta. 13 (1968) 1351–1358. doi:10.1016/0013-4686(68)80062-3.
[72] M.-W. Xu, S.-J. Bao, H.-L. Li, Synthesis and characterization of mesoporous nickel oxide for electrochemical capacitor, J. Solid State Electrochem. 11 (2006) 372–377. doi:10.1007/s10008-006-0155-6.

[73] J. Cheng, G.P. Cao, Y.S. Yang, Characterization of sol-gel-derived NiOxxerogels as supercapacitors, J. Power Sources. 159 (2006) 734–741. doi:10.1016/j.jpowsour.2005.07.095.
[74] A. Kumar Rai, L. Tuan Anh, C.J. Park, J. Kim, Electrochemical study of NiO nanoparticles electrode for application in rechargeable lithium-ion batteries, Ceram. Int. 39 (2013) 6611–6618. doi:10.1016/j.ceramint.2013.01.097.
[75] W. Xing, F. Li, Z.F. Yan, G.Q. Lu, Synthesis and electrochemical properties of mesoporous nickel oxide, J. Power Sources. 134 (2004) 324–330. doi:10.1016/j.jpowsour.2004.03.038.
[76] B.E. Conway, M.A. Sattar, Electrochemistry of the nickel oxide electrode, J. Electroanal. Chem. Interfacial Electrochem. 19 (1968) 351–364. doi:10.1016/S0022-0728(68)80098-1.
[77] Y. Matsumoto, E. Sato, Electrocatalytic properties of transition metal oxides for oxygen evolution reaction, Mater. Chem. Phys. 14 (1986) 397. http://www.sciencedirect.com/science/article/pii/0254058486900453.
[78] E. Arciga-Duran, Y. Meas, J.J. Pérez-Bueno, J.C. Ballesteros, G. Trejo, Effect of oxygen vacancies in electrodeposited NiO towards the oxygen evolution reaction: Role of Ni-Glycine complexes, Electrochim. Acta. 268 (2018) 49–58. doi:10.1016/j.electacta.2018.02.099.
[79] R.L. Doyle, M.E.G. Lyons, The oxygen evolution reaction: Mechanistic concepts and catalyst design, in: Photoelectrochem. Sol. Fuel Prod. From Basic Princ. to Adv. Devices, 2016: pp. 41–104. doi:10.1007/978-3-319-29641-8_2.
[80] M. Bonomo, D. Dini, A.G. Marrani, Adsorption Behavior of I3- and I- Ions at a Nanoporous NiO/Acetonitrile Interface Studied by X-ray Photoelectron Spectroscopy, Langmuir. 32 (2016) 11540–11550. doi:10.1021/acs.langmuir.6b03695.
[81] H. Bode, K. Dehmelt, J. Witte, Zur kenntnis der nickelhydroxidelektrode—I.Über das nickel (II)-hydroxidhydrat, Electrochim. Acta. 11 (1966) 1079–1087. doi:10.1016/0013-4686(66)80045-2.
[82] M.E.G. Lyons, M.P. Brandon, The Oxygen Evolution Reaction on Passive Oxide Covered Transition Metal Electrodes in Aqueous Alkaline Solution. Part 1-Nickel, Int. J. Electrochem. Sci. 3 (2008) 1386–1424.
[83] E.A. Gibson, M. Awais, D. Dini, D.P. Dowling, M.T. Pryce, J.G. Vos, G. Boschloo, A. Hagfeldt, Dye sensitised solar cells with nickel oxide photocathodes prepared via scalable microwave sintering., Pccp. 15 (2013) 2411–2420. doi:10.1039/c2cp43592f.
[84] M.J. Honeychurch, G.A. Rechnitz, Voltammetry of adsorbed molecules. Part 2: Irreversible redox systems, Electroanalysis. 10 (1998) 285–293. doi:10.1002/(SICI)1521-4109(199806)10:7<453.
[85] B.B. Damaskin, O.A. Petrii, Historical development of theories of the electrochemical double layer, J. Solid State Electrochem. 15 (2011) 1317–1334. doi:10.1007/s10008-011-1294-y.
[86] M. Bonomo, D. Dini, A.G. Marrani, R. Zanoni, X-ray photoelectron spectroscopy investigation of nanoporous NiO electrodes sensitized with Erythrosine B, Colloids Surfaces A Physicochem. Eng. Asp. (2017). doi:10.1016/j.colsurfa.2017.04.029.
[87] C.J. Wood, G.H. Summers, C.A. Clark, N. Kaeffer, M. Braeutigam, L.R. Carbone, L. D'Amario, K. Fan, Y. Farré, S. Narbey, F. Oswald, L.A. Stevens, C.D.J. Parmenter, M.W. Fay, A. La Torre, C.E. Snape, B. Dietzek, D. Dini, L. Hammarström, Y. Pellegrin, F. Odobel, L. Sun, V. Artero, E.A. Gibson, A comprehensive comparison of dye-sensitized NiO photocathodes for solar energy conversion., Phys. Chem. Chem. Phys. 18 (2016) 10727. doi:10.1039/c5cp05326a.
[88] D. Dini, F. Decker, G. Zotti, G. Schiavon, S. Zecchin, F. Andreani, E. Salatelli, M. Lanzi, EQCM Characterization of some substituted polyterthiophenes, Electrochim. Acta. 44 (1999) 1911–1917.
[89] D. Dini, F. Decker, G. Zotti, Electrochemical growth of polyalkylthiophenes. In situ characterization of deposition processes, Electrochem. Solid-State Lett. 1 (1998) 217–219.

[90] L. D'Amario, G. Boschloo, A. Hagfeldt, L. Hammarström, Tuning of conductivity and density of states of NiO mesoporous films used in p-type DSSCs, J. Phys. Chem. C. 118 (2014). doi:10.1021/jp504551v.
[91] L. Chernyak, K. Gartsman, D. Cahen, O.M. Stafsudd, Electronic effects of ion mobility in semiconductors: Semionic behaviour of CuInSe2, J. Phys. Chem. Solids. 56 (1995) 1165–1191. doi:10.1016/0022-3697(95)00050-X.